BIOMATERIALS

An engineered cell-laden adhesive hydrogel promotes craniofacial bone tissue regeneration in rats

Mohammad Mahdi Hasani-Sadrabadi[1,2,3], Patricia Sarrion[1], Sevda Pouraghaei[1], Yee Chau[4], Sahar Ansari[1], Song Li[3], Tara Aghaloo[4]*, Alireza Moshaverinia[1,2,3]*

Cell-laden hydrogels are widely used in tissue engineering and regenerative medicine. However, many of these hydrogels are not optimized for use in the oral environment, where they are exposed to blood and saliva. To address these challenges, we engineered an alginate-based adhesive, photocrosslinkable, and osteoconductive hydrogel biomaterial (AdhHG) with tunable mechanical properties. The engineered hydrogel was used as an injectable mesenchymal stem cell (MSC) delivery vehicle for craniofacial bone tissue engineering applications. Subcutaneous implantation in mice confirmed the biodegradability, biocompatibility, and osteoconductivity of the hydrogel. In a well-established rat peri-implantitis model, application of the adhesive hydrogel encapsulating gingival mesenchymal stem cells (GMSCs) resulted in complete bone regeneration around ailing dental implants with peri-implant bone loss. Together, we have developed a distinct bioinspired adhesive hydrogel with tunable mechanical properties and biodegradability that effectively delivers patient-derived dental-derived MSCs. The hydrogel is photocrosslinkable and, due to the presence of MSC aggregates and hydroxyapatite microparticles, promotes bone regeneration for craniofacial tissue engineering applications.

INTRODUCTION

Reconstruction of pathologically damaged craniofacial bones may be accomplished by an array of surgical procedures. Autologous and allogenic bone grafts currently comprise more than 90% of grafts performed each year (*1*, *2*). However, there are several disadvantages associated with these methodologies, such as donor site morbidity, hematoma, inflammation, and the high cost of bone harvesting procedures. Factors such as the completeness of debridement, shape and size of the defect to be filled, patient compliance, and type of graft material used influence the outcome of bone regenerative therapies (*3*). Mesenchymal stem cells (MSCs) have shown promise as an alternative therapeutic option for bone tissue engineering, with several important advantages over bone grafts (*4*, *5*). Studies have confirmed the self-renewal and multilineage differentiation capacities of dental-derived MSCs (*6*, *7*). Furthermore, dental-derived MSCs have shown superior osteogenic properties to those of bone marrow MSCs (BMMSCs) (*6*, *7*). Gingival MSCs (GMSCs) are of special interest as they are easily accessible in the oral cavity and readily found in discarded dental tissue samples (*8*, *9*). The use of an appropriate scaffold biomaterial as a cell delivery vehicle can provide a suitable microenvironment to prolong cell viability and also present essential factors to direct MSC differentiation toward the desired lineages (*10*).

Adhesion and retention at the application site as well as the regenerative properties of the biomaterial are vital factors for successful craniofacial tissue regeneration. However, currently, a major drawback of the reported cell-laden hydrogels for craniofacial tissue engineering is their weak adhesion to the host tissue at the defect site, which limits their regenerative properties. Several types of hydrogel-based adhesives have been used for sealing tissues or coating implants to improve their adhesion to the surrounding tissues (*11*–*13*). However, poor mechanical properties, cell compatibility, and lack of adhesion to the surrounding tissues in wet environments are limitations hindering the successful implementation of these adhesives. Inspired by the superior ability of marine mussels to adhere to wet or moist surfaces, L-dopa amino acid has been identified for its potential to improve adhesion (*14*, *15*). The formation of dopamine (DA)–modified hydrogels with strong adhesion to tissues in the presence of blood or saliva is paradigm shifting due to its ability to maintain hydrogel, and therefore the MSCs within it, in a defect site. In addition, osteoconductive hydrogels have been developed by incorporating various growth factors, such as recombinant human bone morphogenetic protein-2 (rhBMP-2), or hydroxyapatite (HAp) particles to induce osteogenic differentiation (*16*, *17*). Bioactive hydrogel/HAp composites have shown promise for use in bone tissue engineering application (*16*, *17*).

To address the clinical need for a multifunctional biomaterial for craniofacial bone tissue regeneration, here we have engineered a bioinspired, visible-light, crosslinkable adhesive hydrogel with tunable physical properties and ability to direct GMSCs toward osteogenic lineages. To induce osteogenesis, HAp microparticles (MPs) were incorporated into GMSC aggregates, and the resulting HAp MP/GMSC aggregates were encapsulated within the engineered hydrogel. A well-established peri-implantitis model in rats was used to analyze the efficacy and functionality of the engineered cell-hydrogel constructs, confirming the injectability of the hydrogel into the defect site, rapid photopolymerization, adhesion to the surrounding tissues, and ability to promote bone tissue regeneration and repair.

RESULTS

The adhesive and osteoconductive hydrogel described here is based on alginate. Alginate is a polysaccharide found in algae that has been used in a wide variety of biomedical applications, including the encapsulation of cells and sensitive bioactive molecules to facilitate minimally invasive surgeries (*18*, *19*). Alginate can provide a

[1]Weintraub Center for Reconstructive Biotechnology, Division of Advanced Prosthodontics, School of Dentistry, University of California, Los Angeles, Los Angeles, CA 90095, USA. [2]California NanoSystems Institute, University of California, Los Angeles, Los Angeles, CA 90095, USA. [3]Department of Bioengineering, University of California, Los Angeles, Los Angeles, CA 90095, USA. [4]Division of Diagnostic and Surgical Sciences, School of Dentistry, University of California, Los Angeles, Los Angeles, CA 90095, USA. *Corresponding author. Email: amoshaverinia@ucla.edu (A.M.), taghaloo@dentistry.ucla.edu (T.A.)

three-dimensional (3D) scaffold that holds MSCs in a desirable and easily engineered spatial distribution, resulting in a structural organization that can be tailored to resemble specific in vivo microenvironments.

Adhesive hydrogel synthesis and characterization

We synthesized and characterized methacrylated alginate hydrogel based on methods already in the literature (*20*). Next, by incorporation of chemical motifs (DA hydrochloride via carbodiimide bioconjugation) that mimic the structure of L-dopa to modify the crosslinkable methacrylate alginate, we enhanced its adhesive properties. The resulting hydrogel was further modified with a collagen-mimicking short peptide [$(Gly)_4$-Arg-Gly-Asp-Gly-Ser; RGD] to form an alginate-based adhesive hydrogel (AdhHG); Fig. 1A.

AdhHG can be cross-linked via the addition of Ca^{2+}-rich media or by chemical/enzymatic oxidizing of DA residues. Visible-light cross-linkability is highly desirable for command-cure dental applications. To achieve this, eosin Y was used as an initiator, triethanolamine as a coinitiator, and vinyl caprolactam as a catalyst to initiate a photopolymerization reaction through exposure to blue-green light (450 to 550 nm, Xenon source) at 100 mW/cm^2 for 20 s. The resulting hydrogel (Fig. 1B) has a highly porous microstructure with pore sizes on the order of 80 μm (Fig. 1C).

The presence of DA residues was confirmed by the appearance of an ultraviolet (UV)–vis absorption peak at 278 nm (Fig. 1D). The successful chemical modification of the alginate with DA and methacrylate residues was also confirmed by ^{1}H nuclear magnetic resonance (NMR), as shown in Fig. 1E. Our data showed that the adhesive hydrogel system has physical properties (mechanical, swelling, and degradation) that can be tuned by changing the degree of methacrylation (Fig. 1, F and G), photoinitiator concentration, or exposure time. We have optimized the elasticity of the hydrogel for bone tissue engineering applications to an elastic modulus between 22 and 30 kPa. In addition, the reproducibility of the results was tested by comparing the physical (elastic modulus) and biological properties of six batches of adhesive hydrogels that were independently synthesized over a period of 3 months. No significant ($P > 0.05$) variability was found in their mechanical properties, which confirmed batch-to-batch reproducibility (figs. S1 and S2). Freeze-dried hydrogel batches also exhibited a prolonged shelf life of up to 24 months from the date of manufacturing (fig. S3).

To analyze the in vitro biodegradation of the engineered hydrogel, specimens were immersed in phosphate-buffered saline (PBS) solution and human saliva at 37°C, and the amount of weight loss was measured at different time intervals (Fig. 1H). One of the important contributing factors to the success of craniofacial bone regeneration is the adhesion and retention of the cell-laden biomaterial at the defect site (*21*). Hence, ex vivo tests were performed to evaluate the adhesive properties of the selected hydrogels to alveolar bone, gingival tissue, and teeth. The results demonstrated that AdhHG adheres strongly to both hard and soft tissues after being cross-linked, as shown by its adherence to rat gingiva (Fig. 1I), rat calvarial bone and periosteum (Fig. 1J), and human tooth root surfaces (Fig. 1K); in contrast, hydrogel prepared without DA residues failed to demonstrate adhesion to any of the tested substrates. The adhesive properties of AdhHG with different degrees of DA conjugation were further evaluated by performing ex vivo tests of adhesion to rat alveolar bone (Fig. 1L) and porcine gingival tissue. The adhesive hydrogel with a medium degree of DA conjugation exhibited the strongest adhesive properties to porcine gingival tissue (Fig. 1, M and N, and fig. S4). It has been reported that the presence of DA causes formation of strong inter- and intramolecular hydrogen bonding (*22*, *23*). Increasing DA substitution will increase the number of formed intramolecular hydrogen bonds, which causes formation of more brittle hydrogels due to the increase in cross-linking density.

In vivo biocompatibility and biodegradation of adhesive hydrogels

It has been reported that GMSCs have similar differentiation capacities to BMMSCs but surpass BMMSCs for bone tissue engineering applications due to their superior growth properties (*8*, *9*). Therefore, we used human GMSCs in combination with our engineered scaffolds for regenerative/therapeutic applications. Mesenchymal characteristics of extracted cells were checked with flow cytometry for MSC surface markers (CD73, CD146, CD166, and Sca-1), and cells were confirmed to be negative for hematopoietic cell markers (CD31, CD34, and CD45) (*8*, *9*). In vitro cytocompatibility of the developed hydrogels was tested using GMSCs. The hydrogel spheres encapsulated GMSCs at cell density of 2×10^6 cells/ml (Fig. 2A). Modifying alginate with DA and methacrylate anhydride did not affect the cytocompatibility of the hydrogels (viability, >85%) (Fig. 2, B to D).

The in vivo biocompatibility and degradation of the engineered modified alginate-based adhesive hydrogel (AdhHG) were tested in wild-type mice using a subcutaneous implantation model. No signs of lymphocyte (CD3) or macrophage (CD68) infiltration were observed 7 days after subcutaneous implantation (Fig. 2E). On the basis of these results, we do not expect significant ($P > 0.05$) foreign body response to the AdhHG. Comprehensive testing was also performed on the blood of the recipient mice to check for any potential systematic toxicity of the hydrogels. Comparing results to those of mice that received commercially available Alginate–RGD (Alg) hydrogels, there were no significant differences ($P > 0.05$) in blood cells (Fig. 2F). Metabolic screening 7 days after administration of various hydrogels also showed no significant changes ($P > 0.05$) in liver/kidney functions. However, moderate changes in some electrolytes [bicarbonate ($P = 0.03$)] were observed with hydrogels, including methacrylate residues (Fig. 2G).

To study in vivo degradation, specimens with optimized adhesive properties were implanted in wild-type mice subcutaneously. The degradation of the hydrogels was followed for periods of 1 and 6 weeks. Our results showed that more than 50% of the alginate had dissociated after 6 weeks of subcutaneous implantation (Fig. 2H). The biodegradation rate of alginate-based constructs can be further modified by reducing the molecular weight of the alginate backbone via controlled oxidation (*24*). Thus, hydrogels with low oxidation degrees (~2%) will remain intact for more than 6 weeks, whereas highly oxidized versions (~10%) will be absorbed faster (within 1 month).

In vitro osteogenic differentiation of MSC aggregates encapsulated in adhesive hydrogels

To form a hydrogel that is osteoconductive yet free of growth factors, we further modified the engineered adhesive hydrogel with HAp MPs. Spray-dried HAp MPs with an average size of 5.0 μm (specific surface area, ≥100 m^2/g) were used. These MPs are cytocompatible with human and animal stem cells, as reported in previous studies (*25*); it has also been established that HAp particles can induce osteogenic differentiation of stem cells in the absence of any external osteoinductive factors (*26*).

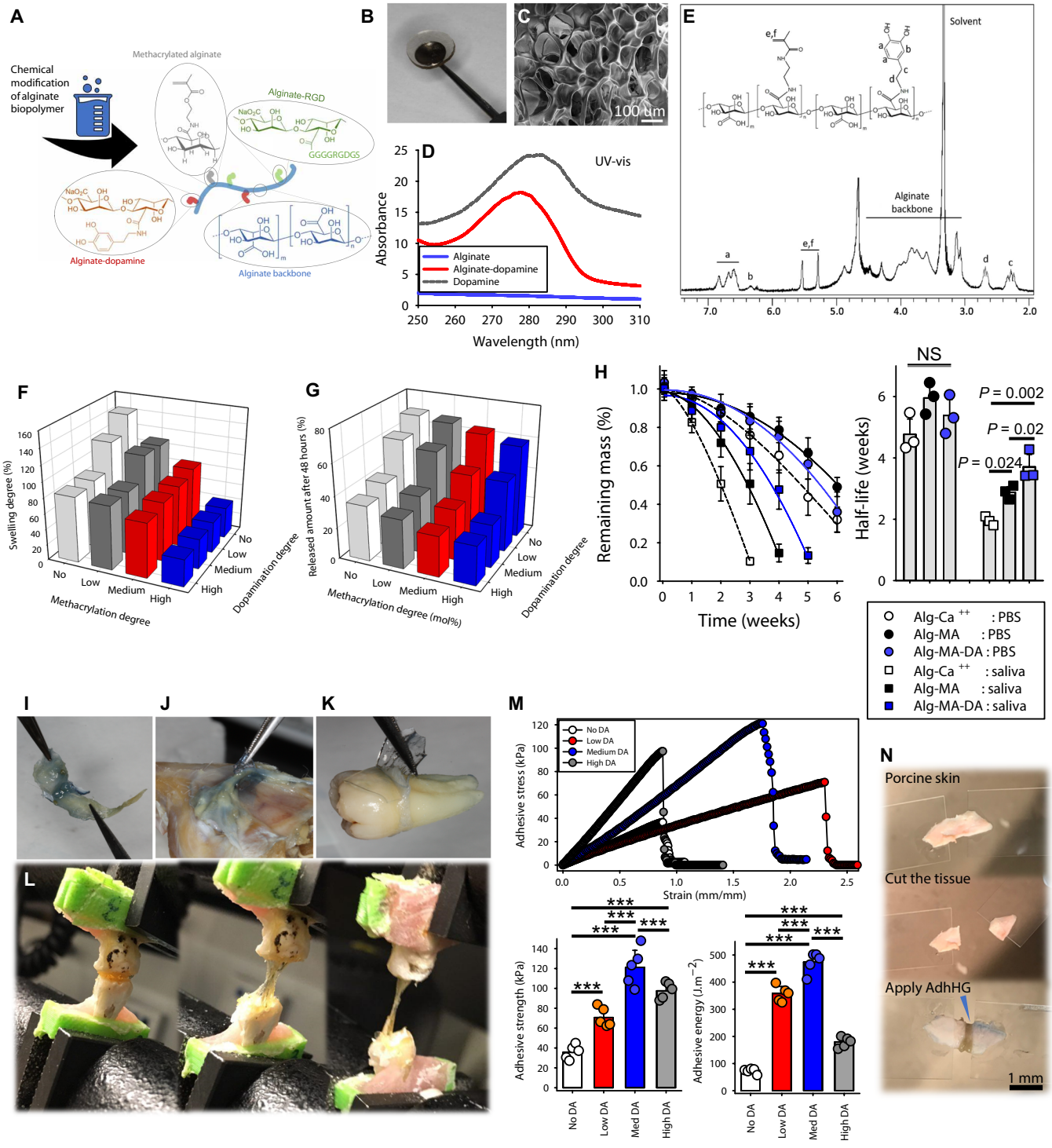

Fig. 1. Adhesive hydrogel synthesis and characterization. (**A**) Schematic illustration of chemical modification of alginate to make alginate-based adhesive hydrogel (AdhHG) that is photopolymerized either via visible light (eosin Y)– or UV (Irgacure 2959)–based photoinitiators. (**B**) Visualization of light-cured synthesized hydrogel and (**C**) its microstructure via scanning electron microscopy. Scale bar, 100 μm. (**D**) UV-vis and (**E**) H-NMR spectra of synthesized AdhHG. Full factorial investigation of methacrylation degree (0 to 22%) and degree of dopamine (DA) conjugation (0 to 4 mol%) on (**F**) swelling degree and (**G**) cumulative amount of release of sample protein [BSA–fluorescein isothiocyanate] after 48 hours ($n = 3$). (**H**) In vitro degradation based on mass loss of the hydrogels with and without presence of dopamine/methacrylate groups after incubation of hydrogels in either PBS or human saliva. The estimated half-life of different formulations is shown on the right ($n = 3$). Photographs illustrating hydrogel adhesiveness to (**I**) rat gingiva, (**J**) rat calvarial bone and periosteum, and (**K**) human tooth root surfaces. (**L**) Sequential images of tensile experiment on rat alveolar bone adhesion. (**M**) Stress-strain curve to identify adhesion strength and adhesion energy to porcine skin ($n = 5$). Sample preparation for adhesion test on porcine skin is shown in (**N**). The data are expressed as means ± SD. The results were statistically analyzed using one-way ANOVA with post hoc analysis. For all tests, ***$P < 0.001$ for differences between samples with different formulations. NS, not significant.

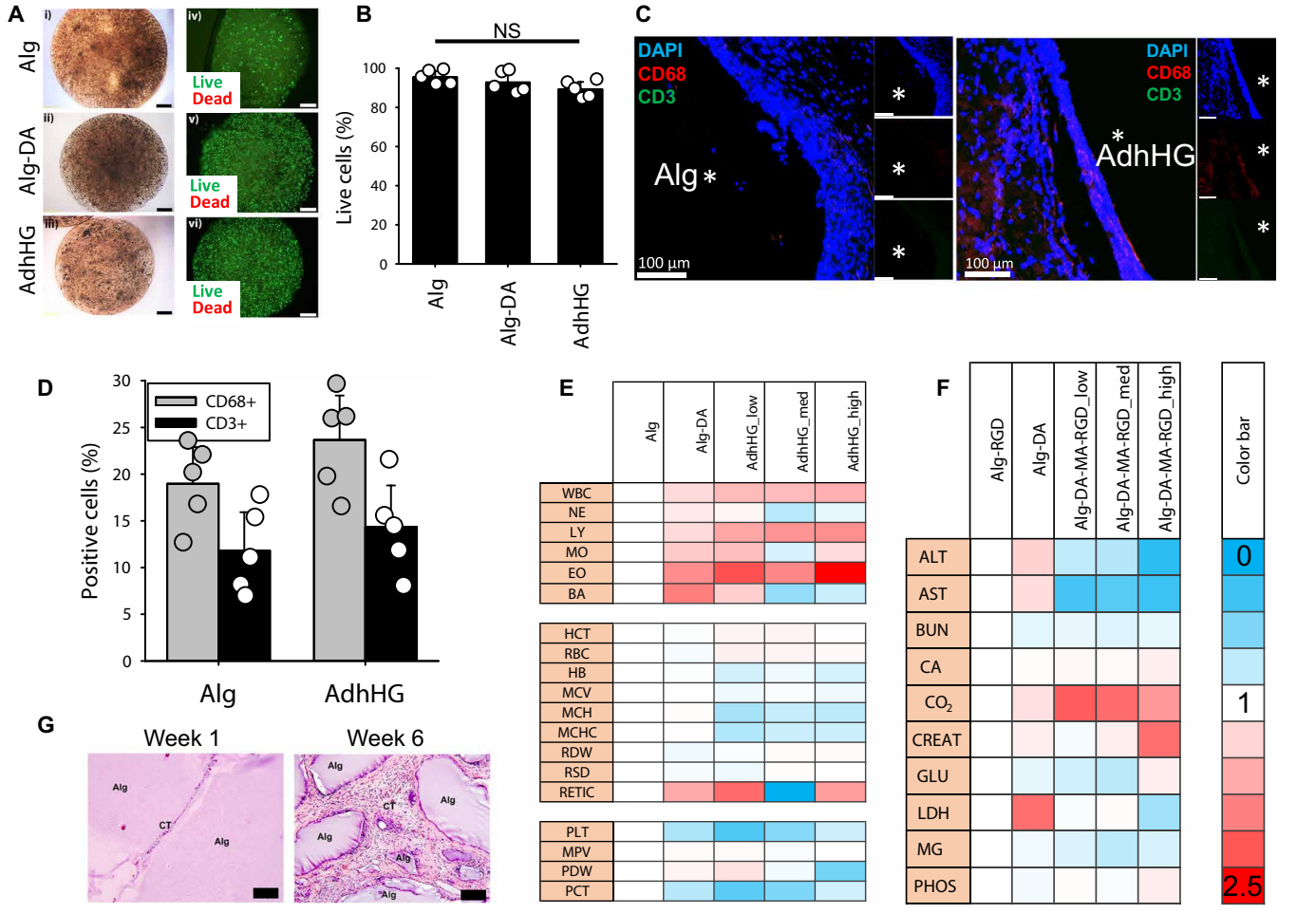

Fig. 2. In vitro cytocompatibility and in vivo biocompatibility of adhesive hydrogel. (**A**) In vitro biocompatibility of encapsulated GMSCs inside hydrogel beads and Live/Dead staining fluorescence images of GMSC-loaded alginate RGD, alginate-dopamine, and AdhHG hydrogels. Scale bars, 500 μm. (**B**) Quantitative Live/Dead results after 1 week of culturing in standard stem cell media. ($P > 0.05$; $n = 5$). (**C**) In vivo biocompatibility of designed hydrogels. Immunostaining of hydrogel boundaries 7 days after subcutaneous implantation in mice (* indicates hydrogel). DAPI, 4′,6-diamidino-2-phenylindole. Scale bars, 100 μm. (**D**) Evaluation of macrophages (CD68) and lymphocytes (CD3) infiltration surrounding the hydrogel implants ($n = 5$). (**E**) Whole-blood analysis of mice after implantation with various hydrogel formulations. Values were normalized to those for Alg-RGD. White blood cells: WBC (white blood cells), NE (neutrophils), LY (lymphocytes), MO (monocytes), EO (eosinophils), BA (basophils). Red blood cells: HCT (hematocrit), RBC (red blood cells), HB (hemoglobin), MCV (mean corpuscular volume), MCH (mean corpuscular hemoglobin), MCHC (mean corpuscular hemoglobin concentration), RDW (red cell distribution width), RSD (reflex sympathetic dystrophy syndrome), RETIC (reticulocytes). Platelets: PLT (platelet count), MPV (mean platelet volume), PDW (platelet distribution width), and PCT (plateletcrit). (**F**) Comprehensive metabolic screening of mice after implantation with various hydrogel formulations. Values were normalized to those for Alg-RGD. Liver function assessment: ALT (alanine aminotransferase), AST (aspartate aminotransferase), BUN (blood urea nitrogen), LDH (lactate dehydrogenase). Kidney function assessment: CREAT (creatinine), GLU (glucose). Electrolytes: CA (calcium), CO_2 (carbon dioxide), MG (magnesium), and PHOS (potassium). (**G**) H&E staining analyzing degradation of the engineered adhesive hydrogel after 1 or 6 weeks of subcutaneous implantation in mice. CT, connective tissue; Alg, unresorbed adhesive alginate hydrogel. Scale bars, 200 μm.

HAp particles at concentrations <5 weight % (wt%) were incorporated into the hydrogel without causing notable aggregation, as assessed using scanning electron microscopy (fig. S5A). The presence of HAp particles enhances the shear-thinning properties of the hydrogel, which can be photocrosslinked upon injection into the defect site (*27*). We confirmed that the HAp particles induced osteogenic differentiation of human GMSCs by culturing them in either standard stem cell maintenance or osteogenic induction media for 4 weeks, after which we evaluated multiple osteogenic markers and stained for calcium-mineralized contents (fig. S5B). The addition of HAp MPs to the adhesive hydrogel induced osteogenesis, and it also enhanced the mechanical properties of the tissue construct while strengthening its interfacial properties (fig. S1). The rheological properties of AdhHG containing 2 wt% HAp were also studied to assess the recovery and injectability of the designed formulation (fig. S6).

To more effectively induce osteogenesis and also take advantage of the beneficial effects of cell-cell contact, we developed stem cell aggregates into which we incorporated HAp MPs before encapsulating these aggregates in AdhHG (Fig. 3A). Studies have shown that the presence of particles like HAp MPs within stem cell aggregates can differentially modulate the gene and protein expression patterns of several differentiation markers without adversely affecting cell viability (*28*). Therefore, it is possible to incorporate MPs like the HAp MPs used here within 3D stem cell aggregates to control the spatial presentation of extracellular environmental cues (soluble factors, extracellular matrix, and intercellular adhesion molecules) to direct MSC

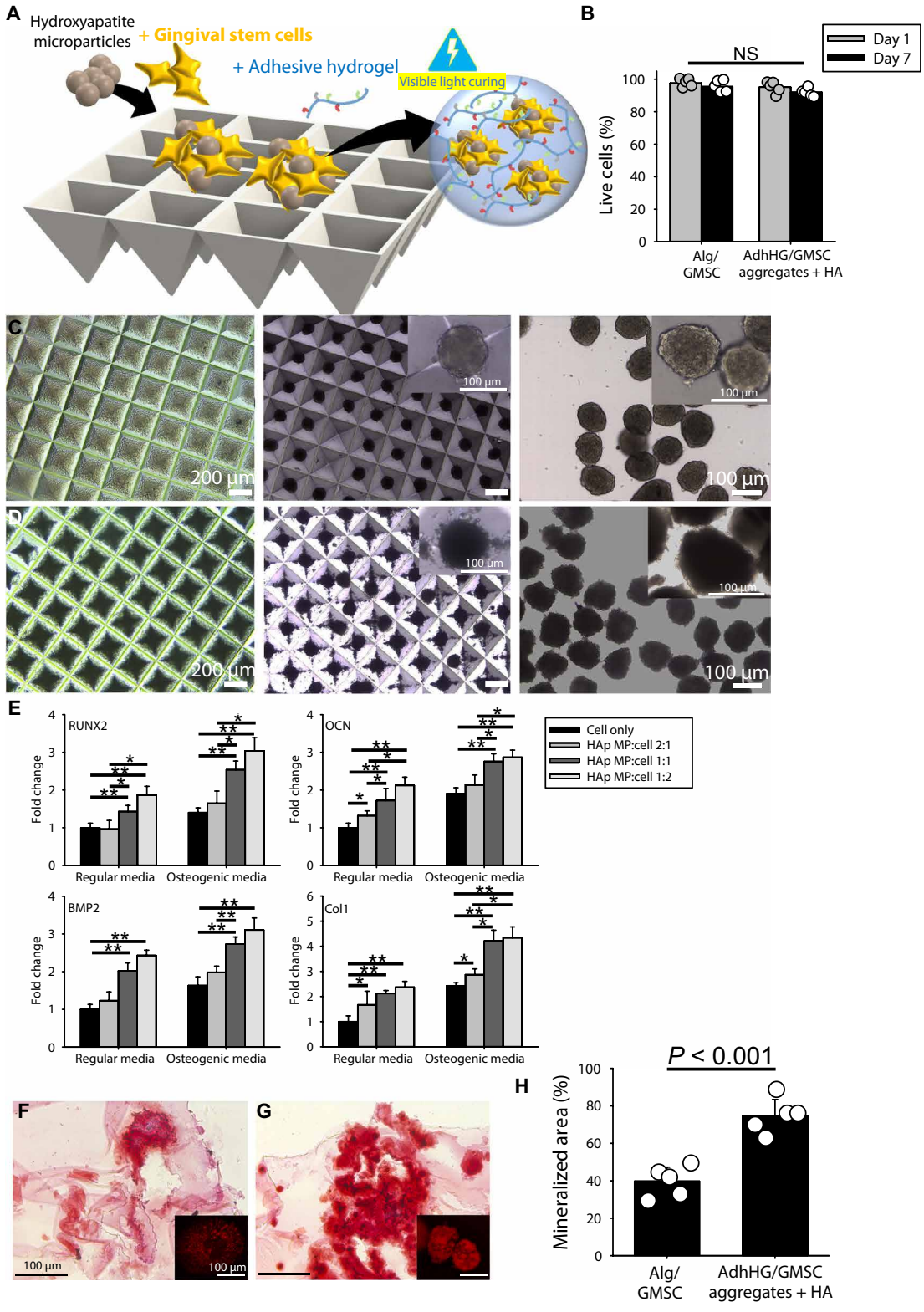

Fig. 3. In vitro osteogenesis of stem cell aggregates encapsulated in adhesive hydrogel. Encapsulated cell aggregates in adhesive hydrogel promote osteogenic differentiation. (**A**) Schematic of the forced aggregation process to prepare GMSC and hydroxyapatite (HA) aggregates. (**B**) Viability (quantitative Live/Dead assay) of single cells and cell aggregates after 1 and 7 days of culture in control hydrogel (Alg-RGD; $n = 5$). Formation of cell GMSC aggregates (**C**) without and (**D**) with HAp MPs (cell:HAp 1:1) inside microwells immediately after seeding (left columns) and after 24 hours of culture (middle columns). Spheroids were removed from the wells and maintained in suspension culture (right columns). (**E**) qPCR demonstrating effects of different HAp MP:cell ratios on expression of osteogenic genes ($n = 3$). Alizarin red staining of single cells (**F**) and GMSC aggregates (**G**) encapsulated in AlgHG after 4 weeks of culturing in osteogenic media. Insets are xylenol orange staining under the same conditions. (**H**) Quantitative measurement of mineralization. Data are expressed as means ± SD. The results were statistically analyzed using one-way ANOVA with post hoc analysis. For all tests, $^{*}P < 0.05$ and $^{**}P < 0.01$ for differences between samples with different formulations.

differentiation and fate determination in tissue engineering applications while providing a high biocompatibility (Fig. 3B). Here, a forced aggregation technique was used to form monodisperse aggregates from GMSCs and HAp MPs (Fig. 3), mimicking the cell-cell contact found in bone tissue, which can induce osteogenesis. Each cell aggregate sample contained 800 to 1200 GMSCs and had an average diameter of 150 ± 5 μm (Fig. 3, C and D). Different ratios of HAp MPs to GMSCs (1:2, 1:1, and 2:1) were tested. Our results suggested that the viability and metabolic activity of stem cell aggregates were not affected by the presence of HAp (up to 2 HAp per cell) (Fig. 3B). These

aggregates were then dispersed in AdhHG and cross-linked to form cell-laden hydrogels.

Lineage specification of cells examined after 4 weeks of culturing either in standard or osteogenic media showed up-regulation of osteogenic markers (*RUNX2*, *OCN*, *BMP-2*, and *Col I*) via polymerase chain reaction (PCR) analysis (Fig. 3E and figs. S7 and S8). Alizarin red and xylenol orange staining demonstrated osteogenic differentiation of encapsulated GMSCs (Fig. 3, F to H, and fig. S9). Increasing the ratio of HAp MPs to MSCs enhanced the osteogenesis, but no significant difference ($P > 0.05$) was observed in the amount of osteogenic differentiation in comparison to constructs with a 1:1 MP:MSC ratio. Therefore, we used a 1:1 ratio in further studies for optimized cell viability and osteogenesis. Our data confirmed that combining GMSC aggregates with HAp MPs significantly ($P < 0.001$) increased the osteogenic differentiation of encapsulated MSCs in AdhHG biomaterial in comparison to single-cell encapsulations (Fig. 3G). Encapsulated GMSCs and aggregates in alginate-based hydrogels retained their viability (<8% reduction in viability) for a week after injection using an 18-gauge needle, as analyzed after 1 and 7 days of in vitro culturing in standard stem cell culture media using live/dead staining assay (Fig. 3B).

In vivo bone regenerative properties of adhesive hydrogels

We used an ectopic bone formation model to test the intrinsic osteogenic properties of the constructs and the in vivo functionality of the designed hydrogel. Immunocompromised mice were subcutaneously injected into the dorsal surface of nude mice with cell-free or cell/aggregate-laden hydrogels of different formulations, and the mice were examined 8 weeks after implantation. Whole-animal x-ray imaging confirmed ectopic osteogenesis and revealed that the optimized stem cell–laden hydrogels (AlgHG/HAp) formed mineralized nodules with similar density to native bone (Fig. 4A). Three-dimensional reconstruction and density mapping of micro–computed tomography (micro-CT) results quantified the amount of mineralization for each hydrogel system. As shown in Fig. 4B, even in the absence of HAp MPs, partial mineralization was achieved upon hydrogel injection due to the presence of DA residues. It has been reported that the presence of DA in biomaterials can accelerate mineralization by promoting the formation of amorphous calcium phosphate from ions available in bodily fluids (*29*). However, a much greater degree of mineralization occurred when the osteogenic DA-containing scaffolds were combined with osteoinductive HAp MPs.

There was no significant difference ($P > 0.05$) between the volumes of mineralized nodules formed by single cells and cell aggregates (Fig. 4C). However, our data confirmed that cell aggregates produced significantly ($P < 0.01$) denser, more highly mineralized bone-like tissue than single cells (Fig. 4D). Characterization of the implanted sites was performed using hematoxylin and eosin (H&E) staining of retrieved specimens to further study the contribution of each hydrogel system to the formation of bone-like tissues. Histological staining confirmed the increase in formation of bone-like tissues with GMSC aggregates compared with single-cell loading (Fig. 4, E and F). We also tested the in vivo mineralization ability of hBMMSCs compared with GMSCs (fig. S10). Although there was no significant volumetric difference in the mineralized tissues formed by these cell types ($P > 0.05$), the constructs formed by GMSCs were more highly mineralized (denser) compared with the ones formed by hBMMSCs ($P < 0.01$).

Next, the in vivo functionality of GMSC-laden, visible-light cross-linkable, DA-modified alginate hydrogels (AdhHG) was evaluated using a well-established peri-implantitis model in rats (*30*, *31*). Studies using rodents have confirmed disease development after placement of implant via an increase of biofilm accumulation (*30*, *31*). This approach is used to reproduce peri-implantitis in human because this model induces changes in the peri-implant tissues similar to those observed in human periodontal and peri-implant disease (apical migration of junctional epithelium and bone loss) (*30*). This clinically relevant model is developed by inoculating titanium dental implants with *Aggregatibacter actinomycetemcomitans* before implant placement. Studies have confirmed that the presence of *A. actinomycetemcomitans* bacteria on the surface of the implant will generate peri-implant bone loss and soft tissue inflammation around the implants (*16*). A titanium dental implant was placed in the diastema between the rat maxillary incisors and molars. Subsequently, the gingival tissues were harvested and GMSCs were isolated according to the methods published in the literature (*17*, *32*). Rat GMSC aggregates and HAp MPs were encapsulated in the AdhHG. Three weeks after placing the implants, we confirmed the presence of peri-implantitis (inflammation and bleeding at the implant site) by clinical examination and micro-CT analysis, which showed bone loss around the implants inoculated with *A. actinomycetemcomitans* bacteria. Subsequently, GMSC-laden adhesive alginate hydrogels were injected into the bony defect sites around the implants (Fig. 5A). Our clinical and micro-CT data demonstrated that adhesive hydrogel containing GMSC aggregates/HAp MPs completely filled the bony defects at the peri-implantitis sites, rescuing the implants in all the experimental rats (Fig. 5B). The amounts of bone regeneration/repair were assessed at 4 and 8 weeks after injection using micro-CT analysis. A statistically significant difference ($P < 0.05$) was observed when GMSC aggregates were used in comparison to the single-cell approach (Fig. 5, C and D). Implant survival and the amount of recovered bone were substantially higher ($P < 0.001$) when the adhesive hydrogel formulation (AdhHG) was applied. Quantifying the expression of inflammatory [tumor necrosis factor–α (TNF-α)] and anti-inflammatory [interleukin-10 (IL-10)] cytokines at different time intervals after treatment (Fig. 5E) confirmed that sustained reduction in local inflammation was achieved by the GMSC-laden adhesive hydrogel constructs.

DISCUSSION

The increased prevalence of bone disorders coupled with developments in regenerative medicine makes bone tissue engineering an attractive option to treat bone defects (*33*). Despite the plethora of available approaches, techniques such as bone grafts used to repair bone defects remain inefficient and limited due to pain, morbidity, insufficient bone available, potential for hematoma formation, risk of inflammation, and high cost of surgical intervention. The ability of MSCs to differentiate into many different types of specialized cells along with their extensive distribution in many adult tissues makes them an advantageous alternative therapeutic for use in tissue engineering. MSCs are multipotent cells with the ability of giving rise to different lineages based on the environmental signals they receive (*34*). MSCs reside in a wide spectrum of postnatal tissue types, and they have been successfully isolated from several orofacial tissues (*35*). Studies have confirmed the self-renewal and multilineage differentiation capacity of dental-derived MSCs and superior osteogenic properties in comparison to BMMSCs (*36*, *37*).

Biomaterials are widely used as cell delivery vehicles to direct stem cell differentiation toward desired phenotypes (*37*, *38*). Adhesion and retention of the biomaterial at the application site and its

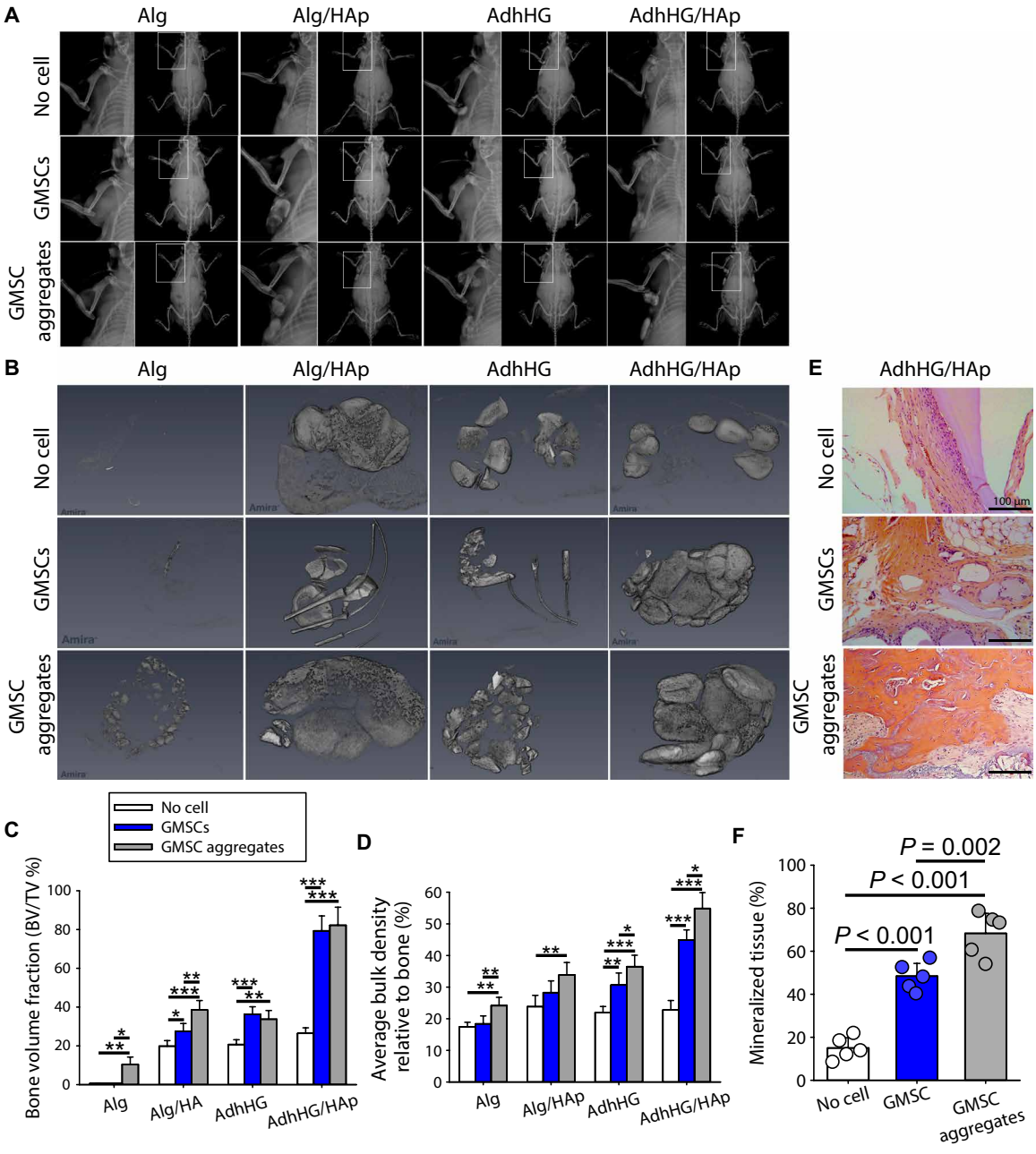

Fig. 4. In vivo analyses of bone regeneration 8 weeks after subcutaneous implantation in immunocompromised mice. (**A**) Faxitron digital in vivo 2D radiographs of subcutaneously implanted hydrogels in the absence (upper panels) or presence of ca. 4×10^6 human GMSCs (middle panels) or an equal number of cells in aggregate form (±HA) (lower panels) per milliliter of Alg (alginate-RGD) ± 2 wt% HAp or AdhHG (±2 wt% HA). Boxed region is shown at higher magnification on the left in each column. (**B**) 3D reconstruction of micro-CT imaging of implanted hydrogels loaded with GMSCs, GMSC aggregates, or no cells. (**C**) Quantified relative mineralized density as normalized to mouse bone density and (**D**) bone volume (BV) fraction measurement derived from BV/total implanted volume (TV). (**E**) H&E staining of formulations of adhesive hydrogels with GMSCs, GMSC aggregates, or no cells 8 weeks after subcutaneous implantation in nude mice. (**F**) Quantified mineralized tissue from (E). The presented data are expressed as means ± SD ($n = 5$). The results were statistically analyzed using one-way ANOVA with post hoc analysis. For all tests, $^*P < 0.05$, $^{**}P < 0.01$, and $^{***}P < 0.001$ for differences between samples with different formulations.

regenerative properties are vital factors for successful bone tissue regeneration. The major drawbacks of previously reported cell-laden biomaterials for periodontal regeneration are weak adhesion to the tissue at the defect site, poor mechanical strength, fast/uncontrolled degradation, and absence of regenerative properties (*38*, *39*). Osteoconductive hydrogels developed by incorporating growth factors and bioactive particles or by exploiting inherent properties of the hydrogel material to induce osteogenesis unfortunately do not contain all desired regenerative properties.

The adhesive hydrogel that we developed can be delivered in a minimally invasive manner to fill a craniofacial bone defect site. The hydrogel adheres strongly to the surrounding orofacial tissues (in the

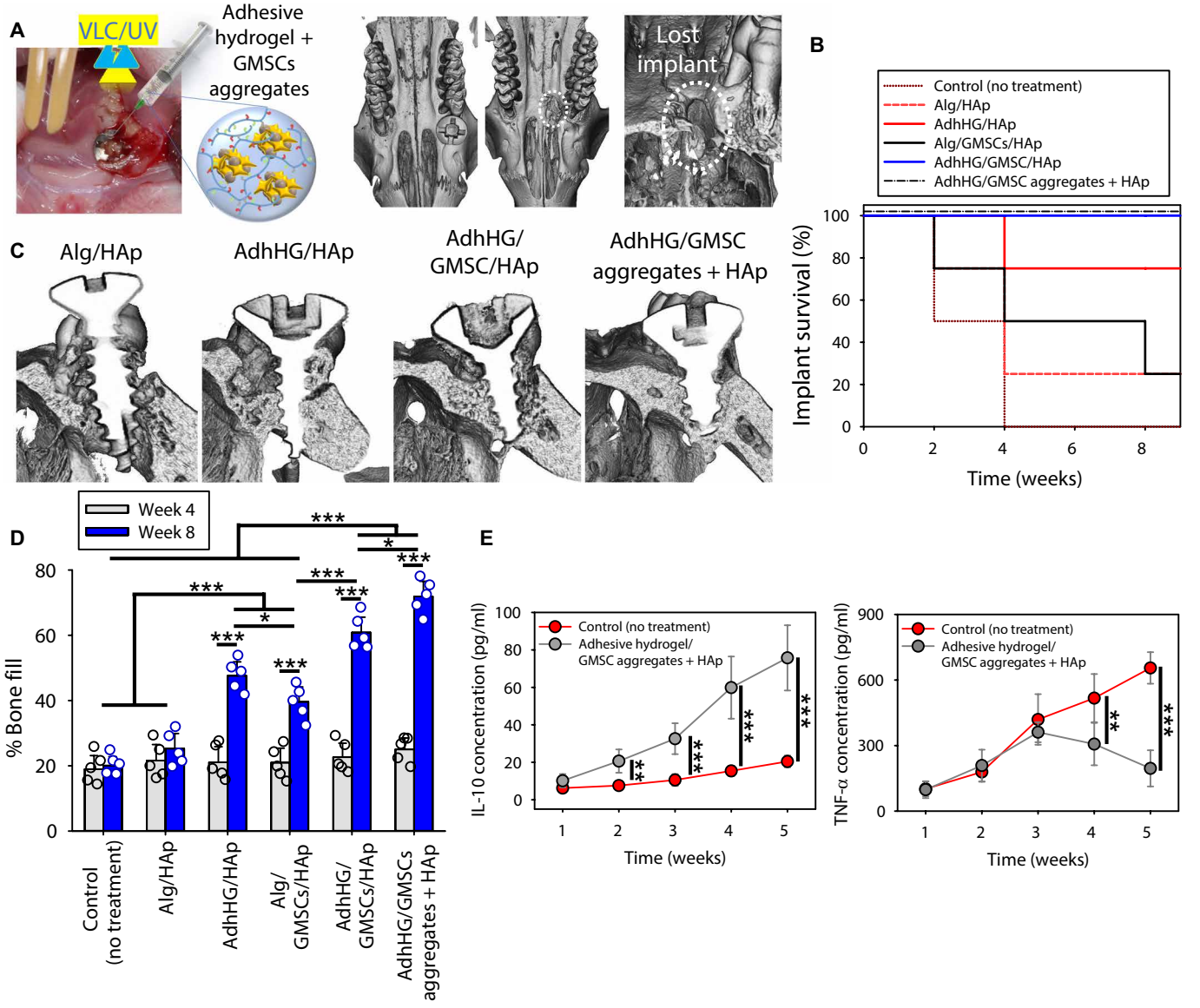

Fig. 5. GMSC-mediated bone repair and regeneration in a rat model of peri-implantitis. (**A**) Photograph, schematic, and 3D micro-CT images of development of a rat model of *A. actinomycetemcomitans*–induced peri-implantitis. *A. actinomycetemcomitans*–coated titanium dental implants caused formation of peri-implantitis. Light-curable adhesive hydrogels with different formulations were injected into the defect, and healing was assessed at various time points afterward. (**B**) Survival of titanium dental implants was assessed over a period of 8 weeks ($n = 4$). Dashed white circles indicate the location of a lost implant. (**C**) 3D micro-CT images of animals treated with optimized formulation of adhesive or control hydrogels with or without cells at 8 weeks after implantation ($n = 5$). (**D**) Quantitative analysis of the amounts of bone fill at the peri-implant defect site 4 and 8 weeks after implantation. (**E**) Quantification of anti-inflammatory (IL-10) and inflammatory (TNF-α) cytokines at different time intervals (1, 2, 3, 4, and 5 weeks) after implantation ($n = 4$). The presented data are expressed as means ± SD. The results were statistically analyzed using one-way ANOVA with post hoc analysis. For all tests, $^{*}P < 0.05$, $^{**}P < 0.01$, and $^{***}P < 0.001$ for differences between samples with different formulations.

presence of saliva and blood) and provides sites for cellular attachment. It has favorable mechanical properties and a desirable degradation rate for bone tissue repair. Although the developed hydrogels are relatively soft (22 to 30 kPa) compared with other materials used to promote osteogenic differentiation, it has been reported that stiffness of cross-linked collagen matrices (collagenous bone) is about 25 to 40 kPa. Engler *et al.* (*40*) reported that osteogenic markers are highly expressed when cells are cultured on 34 kPa gels, whereas other reports confirm that hydrogels with stiffness of 30 to 50 kPa can promote osteogenic differentiation of MSCs (*33*). Much softer hydrogels (10 kPa hyaluronic acid) can promote osteogenesis if supplemented with other signals (*34*). Here, our hydrogel platform provides strong cell adhesion through DA and RGD residues in addition to presenting osteoinductive HAp, which can promote osteogenic differentiation.

To improve host-tissue adhesion, the alginate hydrogel was chemically functionalized with DA, methacrylate, and a cell-adhesive peptide while preserving its distinct physical and regenerative properties. These modifications produced strong adhesion to hard (alveolar bone) and soft tissues including gingival tissues or skin, even in the presence of blood/saliva. Most of the previously developed adhesive hydrogels are not sufficiently adherent to oral tissues (for example, gelatin-based hydrogels), cannot load stem cells (for example, cyanoacrylate

adhesive), or are not osteoinductive (*35*). Moreover, protein-based adhesives such as gelatin-methacrylate (*36*) and fibrin glue are not stable in the presence of human saliva. In contrast, our engineered adhesive hydrogel is stable in the presence of saliva and provides strong adhesion while being more stable than the competitors in a very dynamic oral environment.

Our engineered hydrogel can be injected into a bony defect site through the application of shear stress during injection and afterward can be quickly set through photocrosslinking (*27*). The injected hydrogel can be further stabilized by applying visible light using a dental light cure unit to induce chemical cross-linking with the surrounding tissues, enhancing the hydrogel's mechanical properties and promoting retention at the defect site. The adhesive hydrogel can readily fill the defect site, providing a proper fit and interface between the hydrogel and surrounding tissue. The developed hydrogel was used to deliver dental-derived stem cells, including GMSC aggregates containing osteoinductive MPs. In vitro and in vivo safety, efficacy, and functionality were studied using optimized hydrogel formulations to effectively deliver patient-derived dental-derived MSCs and promote high-quality craniofacial bone regeneration in a well-established peri-implantitis model.

Limitations of the study include the lack of real-time in vivo assessment of hydrogel degradation and new bone formation, which can help identify the optimized physical properties of the hydrogel formulation (*37*). Moreover, single-cell analysis of recovered tissue using various methods like mass cytometry (*38*) can also highlight the role of engineered adhesive biomaterials and encapsulated stem cell aggregates. It has been reported that extracellular matrix–derived scaffolds can trigger a tissue-reparative T cell immune response in mice with injured tissues (*39*). Although our developed hydrogel can help regenerate bone tissue in oral cavity, further optimization of these materials is required to manipulate their interaction with the immune system in the damaged tissue to promote tissue repair (*41*). Our results show that our designed hydrogels have a limited crosstalk with immune cells; however, we believe that by further tuning of our hydrogel platform, we can manipulate this interaction in a constructive way. Another limitation of this study is that our investigations have been performed on small animals (mice and rats), necessitating testing of the functionality of the proposed strategy in a larger animal model such as pigs before moving toward clinical translation of the findings.

In summary, we have developed a bioinspired adhesive hydrogel MSC delivery system with tunable mechanical properties and biodegradability. The hydrogel is photocrosslinkable and promotes bone regeneration for craniofacial tissue engineering applications, demonstrated here in rodents. Thus, our findings support further use of the engineered biologically active and adhesive biomaterial as a next-generation biomaterial for bone tissue engineering.

MATERIALS AND METHODS

Study design

The main goal of our study was to design optimized hydrogels for craniofacial applications. We developed AdhHG, a marine mussel-inspired, adhesive, light-curable hydrogel with osteoinductive properties. To assess the safety of AdhHG in mice, tissue and blood samples were collected for histological evaluation, complete blood count, and blood biochemistry test. After synthesizing, optimizing, and validating the main physical and biological properties, we fabricated rat or human GMSC aggregates with incorporated HAp MPs and encapsulated them in AdhHG. Quantitative PCR (qPCR) analysis was used to study osteogenic differentiation of the encapsulated stem cells in vitro. To test the potential of the regenerating lost bone in a clinically relevant model, titanium dental implants were inoculated with *A. actinomycetemcomitans* before placement of implant in rats. For these in vivo experiments, virgin male and female Sprague-Dawley rats were used ($n = 5$). A titanium dental implant was placed in the diastema between the rat maxillary incisors and molars. *A. actinomycetemcomitans* bacteria on the surface of the implant generated peri-implant bone loss and caused soft tissue inflammation around the implants. After creation of bone loss near the implant, we injected our hydrogels with five different formulations to study the possibility of rescuing the implant by regeneration of the lost bone. Time points (4 and 8 weeks) were chosen to euthanize the animals and test for bone recovery. The inflammatory profile of the peri-implant area was assessed by quantifying the expression of inflammatory (TNF-α) and anti-inflammatory (IL-10) cytokines at different time intervals of 1, 2, 3, 4, and 5 weeks after treatment ($n = 5$). All in vitro experiments were performed in triplicate or quintuplicate. In all experiments, mice or rats were randomly assigned to individual groups of five. Ex vivo and in vitro data were not blinded. The experimenter was blinded to the analysis of all animal-related samples. Neither animals nor samples were excluded from the study. Individual subject-level data for experiments in which $n < 20$ are reported in data file S1.

MSC isolation and characterization

Ten young (16 to 22 years old) healthy male or female individuals undergoing third molar extractions were chosen for extraction of gingival tissues [Institutional Review Board (IRB) approval from the University of California HS 07-00701]. GMSCs were isolated and cultured according to published protocols in the literature. To confirm MSC characteristics of cells, flow cytometric analysis was used to confirm that cells were positive for MSC surface markers CD73, CD146, CD166, and Sca-1 and negative for hematopoietic cell markers CD31, CD34, and CD45 (BD Biosciences, San Jose, CA). Passage 4 cells were used in the experiments (*42*). GMSCs were encapsulated in visible-light crosslinkable adhesive hydrogel.

Chemicals and biologicals

Unless noted otherwise, all chemicals were purchased from Sigma-Aldrich Inc. Glassware was acid cleaned overnight and then thoroughly rinsed with Milli-Q water. Cell culture reagents, solutions, and dishes were obtained from Thermo Fisher Scientific, except as indicated otherwise.

Synthesis of visible-light photocrosslinkable adhesive hydrogel

To make adhesive hydrogels, alginate (Protanal LF 10/60; FMC BioPolymer) was oxidized (2 and 10%) and purified as reported before (*42*). Purified alginate was recovered by freeze drying the solution. Alginate-DA was synthesized by activating the carboxy groups of alginate and reacting them with the amino groups on DA (*43*). Alginate (0.75% w/v) was dissolved in 100 mM 2-(*N*-morpholino) ethanesulfonic acid (MES) buffer at pH 6.1. Nitrogen gas was bubbled through the solution during dissolution to remove oxygen gas. After the overnight stirring at room temperature, *N*-(3-dimethylaminopropyl)-*N*-ethylcarbodiimide hydrochloride (EDC) and *N*-hydroxysuccinimide (NHS) were each dissolved in MES buffer and added to the alginate

solution. After mixing for 15 min, DA was dissolved in MES buffer and added to the alginate reaction mixture (molar ratio of NHS:EDC:DA, 1.2:3:1). The reaction mixture was stirred for 3 hours. The reaction mixture was then dialyzed against PBS (Molecular weight cut-off 6 to 8 kDa) for 3 days and concentrated using 10-kDa Centriprep centrifugal filters by centrifuging at 800*g*. Then, the mixture was freeze dried (55% yield). Incorporation of DA into the alginate was confirmed via UV-visible (NanoDrop) and NMR (300 MHz; Bruker) spectroscopy measurements.

Methacrylated alginate (Alg-DA-MA) was prepared by reacting alginate with 2-aminoethyl methacrylate hydrochloride (AEMA) (*44*). Alg-DA (0.75% w/v) in 100 mM MES buffer (pH 6.5) was reacted with EDC and NHS (3:1 molar ratio) for 15 min. Then, AEMA (molar ratio of NHS:EDC:AEMA, 1.2:3:1) was added to the product, and the solution was stirred at room temperature for 24 hours. The mixture was dialyzed, purified, and characterized as mentioned in the previous section. Methacrylation degree (no, 0 mol%; low, 5 mol%; medium, 12 mol%; high, 22 mol%) and degree of DA conjugation (no, 0 mol%; low, 1 mol%; medium, 4 mol%; high, 8 mol%) were varied to study the effect of these two factors on biophysical properties of the resulted hydrogels. Cell-adhesive alginate, Alg-DA-MA-RGD (AdhHG), was synthesized by coupling amine-terminated $(Gly)_4$-Arg-Gly-Asp-Gly-Ser (G_4RGDGS) peptide to the carboxylic groups of alginate via EDC/NHS chemistry as previously described. Synthesized AdhHG polymer was then lyophilized and stored at −80°C until experimental use.

In addition to storing the lyophilized samples at −80°C, samples were also stored at room temperature (ca. 22°C) for more than 3 months. Hydrogel samples were made using these lyophilized powders and tested for the change in their physical (here, mechanical) and cell compatibility properties to verify the shelf-life stability of the prepared polymers. HAp MPs were used as an inorganic additive (*25*) to rat or human GMSC aggregates to engineer an osteoconductive adhesive hydrogel. We used spray-dried HAp MPs with average size of 5 μm (Fluidinova, S.A., Portugal). A forced aggregation technique was used to form monodisperse (≈80 to 120 μm) spheroids of GMSC aggregates. Briefly, GMSCs were trypsinized into a single cell suspension and AggreWell 400 inserts (STEMCELL Technologies), ca. 1200 of 400 μm × 400 μm pyramid-like wells per insert, were used to form aggregates. Briefly, 1.5×10^6 GMSCs in medium (with and without HAp MPs) were added into AggreWells, and gently centrifuged at 150*g* for 3 min (*45*). After 24 hours of culture, cell aggregates were removed from the wells and mixed with AdhHG to form cell aggregate–laden hydrogels.

To form the osteoconductive alginate hydrogel, we added different ratios of HAp MPs (HA:GMSCs 2:1, 1:1, and 2:1) to the GMSC aggregates. Here, all the HAp-based hydrogels (with and without cell aggregates) present the equal amount of 20 mg of HAp per milliliter of hydrogel. For samples without GMSC aggregates, 20 mg of HAp was used and mixed with the Alg/AdhHG before adding the cells (GMSC dispersion) and formatting the hydrogel. For formulations with GMSC aggregates, the total amount of HAp that was encapsulated within the aggregates (1:1 cell:HAp ratio) was estimated and deduced from the total amount of HAp in control hydrogels in the absence of GMSC aggregates. The difference was then supplemented within the hydrogel to provide the same 2 wt% HAp loading content. So, the total amount of HAp per milliliter of hydrogel was the same in both cases of single cell and cell aggregates.

Encapsulated GMSCs in visible-light, crosslinkable, adhesive hydrogel were cultured in either standard or osteogenic induction medium for 4 weeks. Xylenol orange staining was used to stain deposited mineralized tissue. Changes in expression of osteogenesis-related genes (*RUNX2*, *OCN*, *BMP-2*, and *Col I*) in encapsulated GMSCs in the presence or absence of HAp MPs were studied using qPCR and used to evaluate the osteogenic potential of encapsulated GMSCs.

Batch-to-batch variation of samples was also tested here by synthesizing six batches of the same polymer conjugated (medium AdhHG) over 3 months. Five hydrogel samples were made from each individual batch of freshly prepared polymer with and without incorporation of 5 wt% HAp and tested to identify the variation in their physical (here, mechanical) and cell compatibility properties to verify the reproducibility of the polymer.

Physical characterization of hydrogels

Mechanical properties of alginate-based hydrogels were tested using an Instron mechanical apparatus (Instron, Norwick, MA) under unconfined compression with a strain rate of 1 mm/min. The samples were hydrated in Dulbecco's modifies Eagle's medium (DMEM) before mechanical testing. The elastic (Young's) modulus was calculated on the basis of the slope of the first 10% of strain in the stress-stain curves.

The injectability of the AdhHG/HAp was analyzed using an Instron mechanical tester following the published protocols (*46*, *47*). Briefly, the AdhHG/HAp was added to 1-ml plastic syringes and injected through standard luer lock 18-gauge and 25-gauge needles. The syringe was touched using an upper compressive plate, and the needle was fixed using the lower tensile grip. Injection force overtime was monitored using Bluehill software. Measurements were performed at a flow rate of 2 ml/hour.

An Anton Paar rheometer was used for rheological testing. AdhHG/HAp (2 wt%) was injected between an 8-mm diameter parallel plate with a gap height of 500 μm (*48*). Frequency and shear rate sweeps were performed at 22°C, sweeping angular frequency from 0.1 to 100 rad/s at 0.1% strain and shear strain from 0.01 to 100% at 10 rad/s angular frequency. Recovery testing was conducted at the angular frequency of 10 rad/s by applying 150% strain for 1 min, followed by 1% strain for 2 min to assess the recovery.

To assess the swelling kinetics of the designed hydrogels, the freeze-dried cross-linked hydrogel samples were immersed into the distilled water at 37°C. Weight of each swollen specimen was measured 16 hours later after the removal of the excess surface solution using a filter paper. The swelling degree was calculated according to the formula: Swelling Degree = $100 \times (W_t - W_0)/W_0$, where W_t and W_0 are the weight of the swollen hydrogel at time t (16 hours) and the weight of the unswollen hydrogel on day 0, respectively.

To determine the influence of the microstructure of the hydrogel on its permeability, the release of bovine serum albumin (BSA; 66 kDa) from alginate hydrogels with different formulations was evaluated in PBS solution after 48 hours. A UV spectrophotometer (at 320 nm; Beckman, Brea, CA) was used to analyze the amount of released BSA and was normalized to the initial loading content to calculate the released portion. Moreover, the microstructure of the hydrogels was analyzed using scanning electron microscopy (Zeiss Supra 40VP).

In vitro cytocompatibility studies

Studies were performed in 2D (cell seeding on the hydrogel surface) and 3D (cell encapsulation within the hydrogel) at cell densities ranging from 1×10^6 to 1×10^8 cells/ml. For 2D studies, DA-modified alginate hydrogels were made after exposure to visible light as described

previously, seeded with the cells, and incubated for 14 days. Media were changed twice per week. For 3D cell encapsulation, cells were trypsinized and resuspended in alginate hydrogel containing photoinitiators. Cell-laden alginate hydrogels were made after exposure to visible light, washed three times with PBS, and incubated for 14 days in standard stem cell culture medium. Cell viability was evaluated using calcein-AM/ethidium homodimer Live/Dead assays. For in vitro biodegradation analysis, the engineered hydrogel specimens were immersed in PBS solution at 37°C, and the amount of weight loss was measured at different time intervals (8 hours, 1 week, 2 weeks, 3 weeks, 4 weeks, 5 weeks, and 6 weeks). We also measured the degradation of synthesized hydrogels in human saliva to test the stability of samples in a more realistic condition. To prepare human saliva, unstimulated, whole saliva samples were collected from healthy individuals under institutional IRB-approved protocol. The saliva samples were then homogenized using a tissue homogenizer for 30 s, and bulk debris was removed by centrifugation at 3000 rpm for 15 min at 4°C. The supernatant was collected and filtered using Steriflip 0.22-μm vacuum filtration system (EMD Millipore). The filtrate was stored at −80°C before use. For in vitro biodegradation analysis in saliva, the engineered hydrogel specimens were immersed in PBS solution at 37°C, and the amount of weight loss was measured at different time intervals (8 hours, 1 week, 2 weeks, 3 weeks, 4 weeks, and 5 weeks).

Ex vivo adhesion tests

Ex vivo tests were performed using rat/pig periodontal tissues (alveolar bone and cementum) to evaluate the adhesion of our engineered hydrogel and a commercially available fibrin glue (EVICEL; Johnson & Johnson). Harvested rat/pig/human gingival, alveolar bone, and tooth root samples were used to test the adhesion strength of the selected alginate formulations based on methods reported in the literature, using a modified ASTM F2458-05 standard. Briefly, fresh gingival tissues, alveolar bone, and cementum were obtained and cut into suitable samples (2 mm × 1 mm × 1 mm) and then cut in half ($n = 5$). Tissues were immersed in PBS before testing to prevent drying and then either embedded in 3D-printed ABS blocks (10 mm × 30 mm) or glued to glass slides. Two specimens were placed into an Instron testing machine for tensile loading with a strain rate of 1 mm/min. Hydrogel was administered to the adhesive area and crosslinked with visible light. The hydrogel adhesion strength was determined at the point of detaching.

In vitro osteogenic differentiation assay

Human GMSCs (1×10^6) were encapsulated within adhesive hydrogel and cultured in osteogenic media containing 2 mM *b*-glycerophosphate (Sigma-Aldrich), 100 mM L-ascorbic acid 2-phosphate, and 10 nM dexamethasone (Sigma-Aldrich). To analyze the effects of cell aggregates and presence of HAp MPs on osteogenic differentiation, GMSCs aggregate contained 800 to 1200 GMSCs with an average diameter of 150 ± 5 μm and were fabricated using force aggregation technology. GMSC aggregates with HA/GMSC ratio of 1:1 were tested. About 2×10^6 GMSCs aggregates were encapsulated within adhesive hydrogel and cultured in osteogenic media. After 4 weeks of osteogenic induction, the cultures were stained with xylenol orange. In addition, the expression of *BMP2*, *OSX*, *BSP*, *OPN*, *RUNX2*, *OCN*, and *Col I* was assayed by qPCR analysis. Alginate microspheres without cells were used as a negative control. To perform PCR, encapsulated GMSCs were recovered from hydrogels by digesting the hydrogels using alginate lyase (4 mg/ml) for 15 min on a shaker. Total RNA was isolated using TRIzol reagent. RNA was reverse transcribed, and single-stranded complementary DNA (cDNA) was synthesized using the SuperScript III cDNA Synthesis Kit. Relative gene expression was calculated using the $2^{-\Delta\Delta Ct}$ method, with normalization to the C_t of the housekeeping gene GAPDH (glyceraldehyde 3-phosphate dehydrogenase).

In vivo biodegradation and biocompatibility analyses

The University of California Los Angeles Institutional Animal Care and Use Committee has approved the animal models. For the in vivo biodegradation and biocompatibility tests, subcutaneous implantation was used. Briefly, freshly prepared samples were implanted by injection into individual dorsal subcutaneous pockets. Animals were euthanized, and the constructs and surrounding tissue were explanted and analyzed for biocompatibility after 7, 14, or 28 days using histological and immunohistological evaluations as previously described (*49*, *50*). For in vivo biocompatibility tests, two groups of materials were tested: (i) alginate-RGD and (ii) alginate-based hydrogel (visible-light, crosslinkable, adhesive hydrogel) with optimized modulus of elasticity. Each implant type was followed up for four different time periods: 3, 7, 14, and 28 days ($n = 5$ per group based on power analysis). The biocompatibility of samples was determined on the basis of the presence of inflammatory markers including lymphocytes (CD3) and macrophages (CD68). We also assessed the in vivo degradation of the hydrogels at different time points as explained previously (*49*, *50*). For in vivo degradation, the implants were harvested after 7, 14, and 28 days, and histological evaluation of the remained scaffold area was used to determine the degradation.

GMSC-mediated bone formation: Subcutaneous model

Ex vivo–expanded human GMSC aggregates/HAp MPs (4×10^6) were encapsulated in adhesive hydrogel and implanted subcutaneously (0.5 ml) into the dorsal surface of 5-month-old Beige nude XID III (nu/nu) (Harlan, USA) mice. Eight weeks after surgery, the animals were euthanized, and the amounts of bone regeneration were evaluated through radiographic examination, micro-CT analysis, and histology (H&E staining).

Peri-implantitis model

Thirty virgin male and female Sprague-Dawley rats (2-month-old, 250 to 300 g weight; Harlan Laboratories, Livermore, CA, USA) were used for testing the engineered adhesive hydrogels in vivo under approved animal protocols. We have successfully developed a reproducible biofilm-mediated peri-implantitis model using titanium implants (ACE Surgical Supply, Brockton, MA) to introduce a well-characterized strain of *A. actinomycetemcomitans* biofilm transmucosally into rats. To induce peri-implantitis, titanium implant screws were inoculated in *A. actinomycetemcomitans* solution overnight (*30*). The *A. actinomycetemcomitans* inoculated implants were inserted transmucosally into the existing edentulous ridge of rats' maxilla in the diastema between incisors and molars. Three weeks after surgery, the clinical appearance of peri-implant tissues demonstrated spontaneous bleeding, and ulceration and necrosis were noted on peri-implant tissues of biofilm-inoculated but not sham-inoculated control implants. At this time point, the adhesive hydrogel containing autogenous rat GMSC aggregates/HAp MPs was injected using an 18-gauge needle around the periphery of implants, polymerized using a visible light–curing unit (Paradigm, 3M) for 15 s, and the flap was covered over the implant.

After 2, 4, 6, and 8 weeks postadhesive hydrogel injection, the defect sites were assessed for amounts of bone regeneration. At each time interval, animals were euthanized and subjected to radiographic examination and micro-CT analysis. Animals to be euthanized were given a pentobarbital overdose (200 mg/kg) followed by cervical dislocation. This method was consistent with the recommendations of the Panel on Euthanasia of the American Veterinary Medical Association. Scans were performed at 10-μm resolution using a micro-CT scanner (μCT SkyScan 1172; SkyScan, Kontich, Belgium), and volumetric data were converted to Digital Imaging and Communications in Medicine (DICOM) format and imported into Dolphin Imaging software (Chatsworth, CA) to generate 3D and multiplanar reconstructed images to make linear measurements. The imaged volumes were oriented such that the occlusal plane of the molars was parallel to the axial plane, and the sagittal plane intersected the interproximal surfaces of the molars.

Characterization of proinflammatory cytokine expression at defect sites

At different time intervals (2, 4, 6, and 8 weeks) after implantation, five sterile paper points were placed around the defect sites (under general anesthesia) for at least 30 s, and the concentrations of inflammatory cytokines (TNF-α) and anti-inflammatory cytokines (IL-10) were measured using enzyme-linked immunosorbent assay (ELISA) kits.

Statistical analyses

The Kruskal-Wallis rank sum test, one-way analysis of variance (ANOVA), and two-tailed Student's *t* test were used as appropriate to analyze the data at a significance of α or $P < 0.05$. Quantitative data were expressed as means ± SD. To determine the number of specimens for the proposed experiments, power analysis was conducted on the basis of our preliminary data.

SUPPLEMENTARY MATERIALS

stm.sciencemag.org/cgi/content/full/12/534/eaay6853/DC1

Fig. S1. Batch-to-batch variation of synthesized hydrogels (physical evaluation).
Fig. S2. Batch-to-batch variation of synthesized hydrogels (cellular evaluation).
Fig. S3. Shelf-life evaluation of synthesized hydrogels.
Fig. S4. Adhesive strength of synthesized hydrogels compared with fibrin glue.
Fig. S5. Osteogenic differentiation of GMSCs within adhesive hydrogels.
Fig. S6. Rheological evaluation of adhesive hydrogel.
Fig. S7. Osteogenic gene expression of GMSCs within adhesive hydrogels.
Fig. S8. Growth factor gene expression of GMSCs within adhesive hydrogels.
Fig. S9. Mineralization of single GMSCs and GMSC aggregates encapsulated in adhesive hydrogels.
Fig. S10. In vivo bone formation using single GMSCs and GMSC aggregates encapsulated in adhesive hydrogels.
Fig. S11. In vitro degradation of hydrogels in human saliva.
Data file S1. Primary data.

View/request a protocol for this paper from *Bio-protocol*.

REFERENCES AND NOTES

1. M. E. Elsalanty, D. G. Genecov, Bone grafts in craniofacial surgery. *Craniomaxillofac. Trauma Reconstr.* **2**, 125–134 (2009).
2. S. Bhumiratana, G. Vunjak-Novakovic, Concise review: Personalized human bone grafts for reconstructing head and face. *Stem Cells Transl. Med.* **1**, 64–69 (2012).
3. A. M. Tatara, G. L. Koons, E. Watson, T. C. Piepergerdes, S. R. Shah, B. T. Smith, J. Shum, J. C. Melville, I. A. Hanna, N. Demian, T. Ho, A. Ratcliffe, J. J. J. P. van den Beucken, J. A. Jansen, M. E. Wong, A. G. Mikos, Biomaterials-aided mandibular reconstruction using in vivo bioreactors. *Proc. Natl. Acad. Sci. U.S.A.* **116**, 6954–6963 (2019).
4. H. M. Blau, G. Q. Daley, Stem cells in the treatment of disease. *N. Engl. J. Med.* **380**, 1748–1760 (2019).
5. W. L. Grayson, B. A. Bunnell, E. Martin, T. Frazier, B. P. Hung, J. M. Gimble, Stromal cells and stem cells in clinical bone regeneration. *Nat. Rev. Endocrinol.* **11**, 140–150 (2015).
6. J. Guo, J. Weng, Q. Rong, X. Zhang, S. Zhu, D. Huang, X. Li, S. L. Chen, Investigation of multipotent postnatal stem cells from human maxillary sinus membrane. *Sci. Rep.* **5**, 11660 (2015).
7. G. T.-J. Huang, S. Gronthos, S. Shi, Mesenchymal stem cells derived from dental tissues vs. those from other sources: Their biology and role in regenerative medicine. *J. Dent. Res.* **88**, 792–806 (2009).
8. A. Moshaverinia, C. Chen, K. Akiyama, X. Xu, W. W. Chee, S. R. Schricker, S. Shi, Encapsulated dental-derived mesenchymal stem cells in an injectable and biodegradable scaffold for applications in bone tissue engineering. *J. Biomed. Mater. Res. A* **101**, 3285–3294 (2013).
9. A. Moshaverinia, C. Chen, X. Xu, K. Akiyama, S. Ansari, H. H. Zadeh, S. Shi, Bone regeneration potential of stem cells derived from periodontal ligament or gingival tissue sources encapsulated in RGD-modified alginate scaffold. *Tissue Eng. Part A* **20**, 611–621 (2014).
10. A. Khademhosseini, R. Langer, A decade of progress in tissue engineering. *Nat. Protoc.* **11**, 1775–1781 (2016).
11. H. Yuk, C. E. Varela, C. S. Nabzdyk, X. Mao, R. F. Padera, E. T. Roche, X. Zhao, Dry double-sided tape for adhesion of wet tissues and devices. *Nature* **575**, 169–174 (2019).
12. J. Li, A. D. Celiz, J. Yang, Q. Yang, I. Wamala, W. Whyte, B. R. Seo, N. V. Vasilyev, J. J. Vlassak, Z. Suo, D. J. Mooney, Tough adhesives for diverse wet surfaces. *Science* **357**, 378–381 (2017).
13. A. Shagan, W. Zhang, M. Mehta, S. Levi, D. S. Kohane, B. Mizrahi, Hot glue gun releasing biocompatible tissue adhesive. *Adv. Funct. Mater.* , 1900998 (2019).
14. J. Yu, W. Wei, E. Danner, R. K. Ashley, J. N. Israelachvili, J. H. Waite, Mussel protein adhesion depends on interprotein thiol-mediated redox modulation. *Nat. Chem. Biol.* **7**, 588–590 (2011).
15. J. H. Waite, N. H. Andersen, S. Jewhurst, C. Sun, Mussel adhesion: Finding the tricks worth mimicking. *J. Adhes.* **81**, 297–317 (2005).
16. K. Subramani, R. E. Jung, A. Molenberg, C. H. F. Hammerle, Biofilm on dental implants: A review of the literature. *Int. J. Oral Maxillofac. Implants* **24**, 616–626 (2009).
17. I. M. Diniz, C. Chen, S. Ansari, H. H. Zadeh, M. Moshaverinia, D. Chee, M. M. Marques, S. Shi, A. Moshaverinia, Gingival mesenchymal stem cell (GMSC) delivery system based on rgd-coupled alginate hydrogel with antimicrobial properties: A novel treatment modality for peri-implantitis. *J. Prosthodont.* **25**, 105–115 (2016).
18. O. Chaudhuri, L. Gu, D. Klumpers, M. Darnell, S. A. Bencherif, J. C. Weaver, N. Huebsch, H.-P. Lee, E. Lippens, G. N. Duda, D. J. Mooney, Hydrogels with tunable stress relaxation regulate stem cell fate and activity. *Nat. Mater.* **15**, 326–334 (2016).
19. N. Huebsch, E. Lippens, K. Lee, M. Mehta, S. T. Koshy, M. C. Darnell, R. M. Desai, C. M. Madl, M. Xu, X. Zhao, O. Chaudhuri, C. Verbeke, W. S. Kim, K. Alim, A. Mammoto, D. E. Ingber, G. N. Duda, D. J. Mooney, Matrix elasticity of void-forming hydrogels controls transplanted-stem-cell-mediated bone formation. *Nat. Mater.* **14**, 1269–1277 (2015).
20. S. A. Bencherif, R. W. Sands, D. Bhatta, P. Arany, C. S. Verbeke, D. A. Edwards, D. J. Mooney, Injectable preformed scaffolds with shape-memory properties. *Proc. Natl. Acad. Sci. U.S.A.* **109**, 19590–19595 (2012).
21. M. M. Hasani-Sadrabadi, P. Sarrion, N. Nakatsuka, T. D. Young, N. Taghdiri, S. Ansari, T. Aghaloo, S. Li, A. Khademhosseini, P. S. Weiss, A. Moshaverinia, Hierarchically patterned polydopamine-containing membranes for periodontal tissue engineering. *ACS Nano* **13**, 3830–3838 (2019).
22. L. Han, L. Yan, K. Wang, L. Fang, H. Zhang, Y. Tang, Y. Ding, L.-T. Weng, J. Xu, J. Weng, J. Weng, Y. Liu, F. Ren, X. Lu, Tough, self-healable and tissue-adhesive hydrogel with tunable multifunctionality. *NPG Asia Mater.* **9**, e372 (2017).
23. X. Zhao, M. Zhang, B. Guo, P. X. Ma, Mussel-inspired injectable supramolecular and covalent bond crosslinked hydrogels with rapid self-healing and recovery properties via a facile approach under metal-free conditions. *J. Mater. Chem. B* **4**, 6644–6651 (2016).
24. T. Boontheekul, H.-J. Kong, D. J. Mooney, Controlling alginate gel degradation utilizing partial oxidation and bimodal molecular weight distribution. *Biomaterials* **26**, 2455–2465 (2005).
25. A. K. Gaharwar, S. M. Mihaila, A. Swami, A. Patel, S. Sant, R. L. Reis, A. P. Marques, M. E. Gomes, A. Khademhosseini, Bioactive silicate nanoplatelets for osteogenic differentiation of human mesenchymal stem cells. *Adv. Mater.* **25**, 3329–3336 (2013).
26. J. R. Xavier, T. Thakur, P. Desai, M. K. Jaiswal, N. Sears, E. Cosgriff-Hernandez, R. Kaunas, A. K. Gaharwar, Bioactive nanoengineered hydrogels for bone tissue engineering: A growth-factor-free approach. *ACS Nano* **9**, 3109–3118 (2015).
27. J. M. Townsend, E. C. Beck, S. H. Gehrke, C. J. Berkland, M. S. Detamore, Flow behavior prior to crosslinking: The need for precursor rheology for placement of hydrogels in medical applications and for 3D bioprinting. *Prog. Polym. Sci.* **91**, 126–140 (2019).
28. Y. Wang, X. Yu, C. Baker, W. L. Murphy, T. C. McDevitt, Mineral particles modulate osteo-chondrogenic differentiation of embryonic stem cell aggregates. *Acta Biomater.* **29**, 42–51 (2016).
29. J. Ryu, S. H. Ku, H. Lee, C. B. Park, Mussel-inspired polydopamine coating as a universal route to hydroxyapatite crystallization. *Adv. Funct. Mater.* **20**, 2132–2139 (2010).

30. M. O. Freire, P. P. Sedghizadeh, C. Schaudinn, A. Gorur, J. S. Downey, J.-H. Choi, W. Chen, J.-K. Kook, C. Chen, S. D. Goodman, H. H. Zadeh, Development of an animal model for Aggregatibacter actinomycetemcomitans biofilm-mediated oral osteolytic infection: A preliminary study. *J. Periodontol.* **82**, 778–789 (2011).
31. T. Koutouzis, C. Eastman, S. Chukkapalli, H. Larjava, L. Kesavalu, A novel rat model of polymicrobial peri-implantitis: A preliminary study. *J. Periodontol.* **88**, e32–e41 (2017).
32. T. I. Mitrano, M. S. Grob, F. Carrión, E. Nova-Lamperti, P. A. Luz, F. S. Fierro, A. Quintero, A. Chaparro, A. Sanz, Culture and characterization of mesenchymal stem cells from human gingival tissue. *J. Periodontol.* **81**, 917–925 (2010).
33. X. Lin, Y. Shi, Y. Cao, W. Liu, Recent progress in stem cell differentiation directed by material and mechanical cues. *Biomed. Mater.* **11**, 014109 (2016).
34. R. Li, S. Lin, M. Zhu, Y. Deng, X. Chen, K. Wei, J. Xu, G. Li, L. Bian, Synthetic presentation of noncanonical Wnt5a motif promotes mechanosensing-dependent differentiation of stem cells and regeneration. *Sci. Adv.* **5**, eaaw3896 (2019).
35. A. P. Duarte, J. F. Coelho, J. C. Bordado, M. T. Cidade, M. H. Gil, Surgical adhesives: Systematic review of the main types and development forecast. *Prog. Polym. Sci.* **37**, 1031–1050 (2012).
36. B. Liu, Y. Wang, Y. Miao, X. Zhang, Z. Fan, G. Singh, X. Zhang, K. Xu, B. Li, Z. Hu, M. Xing, Hydrogen bonds autonomously powered gelatin methacrylate hydrogels with super-elasticity, self-heal and underwater self-adhesion for sutureless skin and stomach surgery and E-skin. *Biomaterials* **171**, 83–96 (2018).
37. B. A. Aguado, J. C. Grim, A. M. Rosales, J. J. Watson-Capps, K. S. Anseth, Engineering precision biomaterials for personalized medicine. *Sci. Transl. Med.* **10**, eaam8645 (2018).
38. H. Wu, S. Han, B. Wu, X. Du, Z. Sheng, J. Lin, X. Chen, K. Zhao, V. Bunpetch, Y. Chen, M. Zeng, E. V. Alakpa, Y. Ma, X. Lei, J. Huang, X. Zou, H. Ouyang, Single-cell mass cytometry reveals in vivo immunological response to surgical biomaterials. *Appl. Mater. Today* **16**, 169–178 (2019).
39. K. Sadtler, K. Estrellas, B. W. Allen, M. T. Wolf, H. Fan, A. J. Tam, C. H. Patel, B. S. Luber, H. Wang, K. R. Wagner, J. D. Powell, F. Housseau, D. M. Pardoll, J. H. Elisseeff, Developing a pro-regenerative biomaterial scaffold microenvironment requires T helper 2 cells. *Science* **352**, 366–370 (2016).
40. A. J. Engler, S. Sen, H. L. Sweeney, D. E. Discher, Matrix elasticity directs stem cell lineage specification. *Cell* **126**, 677–689 (2006).
41. M. M. Hasani-Sadrabadi, F. S. Majedi, S. J. Bensinger, B. M. Wu, L.-S. Bouchard, P. S. Weiss, A. Moshaverinia, Mechanobiological mimicry of helper T lymphocytes to evaluate cell–biomaterials crosstalk. *Adv. Mater.* **30**, e1706780 (2018).
42. A. Moshaverinia, C. Chen, K. Akiyama, S. Ansari, X. Xu, W. W. Chee, S. R. Schricker, S. Shi, Alginate hydrogel as a promising scaffold for dental-derived stem cells: An in vitro study. *J. Mater. Sci. Mater. Med.* **23**, 3041–3051 (2012).
43. C. J. Kastrup, M. Nahrendorf, J. L. Figueiredo, H. Lee, S. Kambhampati, T. Lee, S.-W. Cho, R. Gorbatov, Y. Iwamoto, T. T. Dang, P. Dutta, J. H. Yeon, H. Cheng, C. D. Pritchard, A. J. Vegas, C. D. Siegel, S. MacDougall, M. Okonkwo, A. Thai, J. R. Stone, A. J. Coury, R. Weissleder, R. Langer, D. G. Anderson, Painting blood vessels and atherosclerotic plaques with an adhesive drug depot. *Proc. Natl. Acad. Sci. U.S.A.* **109**, 21444–21449 (2012).
44. S. A. Bencherif, R. W. Sands, O. A. Ali, W. A. Li, S. A. Lewin, T. M. Braschler, T.-Y. Shih, C. S. Verbeke, D. Bhatta, G. Dranoff, D. J. Mooney, Injectable cryogel-based whole-cell cancer vaccines. *Nat. Commun.* **6**, 7556 (2015).
45. A. M. Bratt-Leal, R. L. Carpenedo, M. D. Ungrin, P. W. Zandstra, T. C. McDevitt, Incorporation of biomaterials in multicellular aggregates modulates pluripotent stem cell differentiation. *Biomaterials* **32**, 48–56 (2011).
46. R. K. Avery, H. Albadawi, M. Akbari, Y. S. Zhang, M. J. Duggan, D. V. Sahani, B. D. Olsen, A. Khademhosseini, R. Oklu, An injectable shear-thinning biomaterial for endovascular embolization. *Sci. Transl. Med.* **8**, 365ra156 (2016).
47. M. H. Chen, L. L. Wang, J. J. Chung, Y.-H. Kim, P. Atluri, J. A. Burdick, Methods to assess shear-thinning hydrogels for application as injectable biomaterials. *ACS Biomater Sci. Eng.* **3**, 3146–3160 (2017).
48. A. K. Gaharwar, R. K. Avery, A. Assmann, A. Paul, G. H. McKinley, A. Khademhosseini, B. D. Olsen, Shear-thinning nanocomposite hydrogels for the treatment of hemorrhage. *ACS Nano* **8**, 9833–9842 (2014).
49. Y.-C. Chen, R.-Z. Lin, H. Qi, Y. Yang, H. Bae, J. M. Melero-Martin, A. Khademhosseini, Functional human vascular network generated in photocrosslinkable gelatin methacrylate hydrogels. *Adv. Funct. Mater.* **22**, 2027–2039 (2012).
50. Y.-N. Zhang, R. K. Avery, Q. Vallmajo-Martin, A. Assmann, A. Vegh, A. Memic, B. D. Olsen, N. Annabi, A. Khademhosseini, A highly elastic and rapidly crosslinkable elastin-like polypeptide-based hydrogel for biomedical applications. *Adv. Funct. Mater.* **25**, 4814–4826 (2015).

Acknowledgments

Funding: Research reported in this publication was supported by grants from the National Institute of Dental and Craniofacial Research of the NIH (NIDCR/NIH) under award numbers DE023825 to A.M., U24DE026914 to T.A. and A.M., and 1R56DE029157 and (NHLBI/NIH) R01HL117213 to S.L., and the California Institute for Regenerative Medicine (grant number DISC1-10718) to A.M.. The content is solely the responsibility of the authors and does not necessarily represent the official views of the NIH, CIRM, and/or other agency of the State of California. **Author contributions:** M.M.H.-S. and A.M. designed the experiments. M.M.H.-S. and P.S. conducted the polymer synthesis, hydrogel preparation, and characterization experiments. M.M.H.-S., P.S., and S.P. conducted the cell culture experiments. M.M.H.-S., S.P., Y.C., T.A., and A.M. designed, performed, and analyzed the animal studies. All authors performed the data analysis and interpreted the results. M.M.H.-S., S.A., S.L., T.A., and A.M. wrote the manuscript with input from all authors. **Competing interests:** M.M.H.-S., T.A., and A.M. have patent applications (Dental Adhesive Hydrogels and Uses Thereof, U.S. Provisional Patent Application 62/641,147) related to the current study and, thus, may have related financial interests. The other authors declare no potential conflicts of interest with respect to the authorship and/or publication of this article. **Data and materials availability:** All data associated with this study are present in the paper or the Supplementary Materials.

Submitted 10 July 2019
Accepted 14 February 2020
Published 11 March 2020
10.1126/scitranslmed.aay6853

Citation: M. M. Hasani-Sadrabadi, P. Sarrion, S. Pouraghaei, Y. Chau, S. Ansari, S. Li, T. Aghaloo, A. Moshaverinia, An engineered cell-laden adhesive hydrogel promotes craniofacial bone tissue regeneration in rats. *Sci. Transl. Med.* **12**, eaay6853 (2020).

Science Translational Medicine

An engineered cell-laden adhesive hydrogel promotes craniofacial bone tissue regeneration in rats

Mohammad Mahdi Hasani-Sadrabadi, Patricia Sarrion, Sevda Pouraghaei, Yee Chau, Sahar Ansari, Song Li, Tara Aghaloo and Alireza Moshaverinia

Sci Transl Med **12**, eaay6853.
DOI: 10.1126/scitranslmed.aay6853

Building bone with a helpful hydrogel

From a materials' perspective, bone regeneration in craniofacial defects can be challenging, particularly considering the aqueous environment of the oral cavity. Hasani-Sadrabadi and colleagues developed an injectable alginate-based adhesive hydrogel that encapsulated aggregates of gingival mesenchymal stem cells and osteoconductive hydroxyapatite microparticles. In a rat model of peri-implantitis, the hydrogel promoted bone regeneration around dental implants. The hydrogel's biodegradation and mechanical properties could be tuned, suggesting it could be a useful tool for tissue engineering.